ELSEVIER

Collision versus collapse of droplets in coarsening of dewetting thin films

K.B. Glasner[a], T.P. Witelski[b],[*]

[a] *Department of Mathematics, University of Arizona, Tucson, AZ 85721, USA*
[b] *Department of Mathematics and Center for Nonlinear and Complex Systems,*
Duke University, Durham, NC 27708-0320, USA

Available online 12 July 2005

Abstract

Thin films of viscous fluids coating solid surfaces can become unstable due to intermolecular forces, leading to break-up of the film into arrays of droplets. The long-time dynamics of the system can be represented in terms of coupled equations for the masses and positions of the droplets. Analysis of the decrease of energy of the system shows that coarsening, decreasing the number of droplets with increasing time, is favored. Here we describe the two coarsening mechanisms present in dewetting films: (i) mass exchange leading to collapse of individual drops, and (ii) spatial motion leading to droplet collisions and merging events. Regimes where each of mechanisms are dominant are identified, and the statistics of the coarsening process are explained.
© 2005 Elsevier B.V. All rights reserved.

Keywords: Dewetting; Coarsening; Thin films; van der Waals forces; Fluid dynamics; Lubrication models

1. Introduction

For thin films of viscous fluids coating solid surfaces, intermolecular forces between the solid and fluid, such as van der Waals attraction and Born repulsion, are known to produce complex dewetting instabilities [1–6]. Much theoretical work has focused on the details of early-stage linear instability [7–10] as well as late-stage nonlinear pattern formation [2,11–13].

The instabilities cause nearly-uniform fluid layers to break-up, or "dewet", into arrays of large droplets connected by a remaining nano-scale ultra-thin film (UTF). The dynamics leading to the formation of such well-defined co-existing stable states is common in other systems with phase separation. In analogy to spinodal decomposition

* Corresponding author. Tel.: +1 919 660 2841.
  E-mail addresses: glasner@math.arizona.edu (K.B. Glasner), witelski@math.duke.edu (T.P. Witelski).
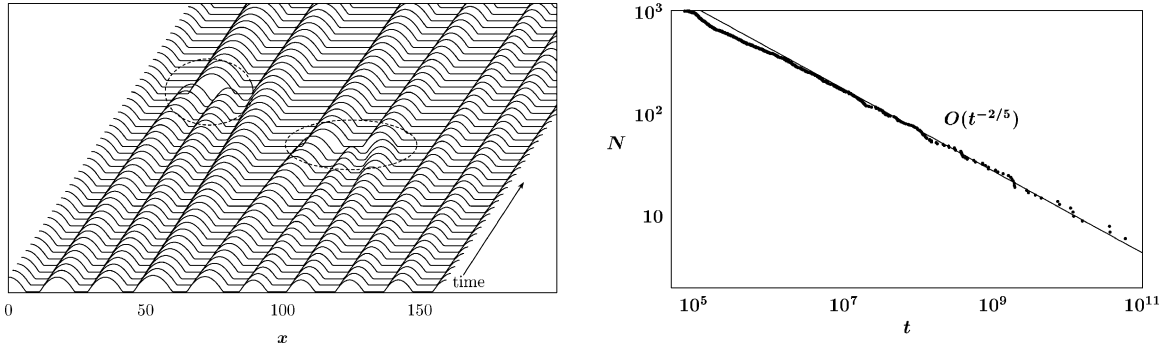
Fig. 1. Numerical simulations of the lubrication model for a dewetting thin film: (left) the evolution of a film at successive times showing droplet collision and collapse events (both circled), (right) the long-time scaling behavior for coarsening of the number of drops $N(t)$ in a large system as a function of time.

described by the Cahn–Hilliard equation [14,15], this evolution in unstable thin films is sometimes called spinodal dewetting [16–18].

In the late stages of the dewetting process, there is a slow evolution of the drops by means of spatial motion and mass flux between drops. In a previous article [19], we showed how the partial differential equation governing the thin film fluid dynamics could be reduced to a system of ordinary differential equations that describe these mechanisms. Over time, these mechanisms can cause the number of droplets to decrease, and the system to "coarsen". Since mass is conserved, this yields a film with fewer, larger drops.

The current paper seeks to quantify the coarsening process and clarify the two mechanisms by which it occurs: (i) collapse of individual drops and (ii) pairwise collision of drops. Fig. 1(left) illustrates both of these mechanisms in a numerical simulation of the governing partial differential equation on a finite domain with no-flux boundary conditions. This paper extends the work initiated by the authors in [19], where only mass exchange driven coarsening, or droplet "collapse", was considered. For systems with large numbers of drops, a scaling law for the droplet number $N(t)$ was found,

$$N(t) = O(t^{-2/5}). \tag{1.1}$$

which was confirmed by numerical simulations, see Fig. 1(right).

Our results run parallel to other studies of dynamical coarsening processes, most notably late-stage phase separation phenomena. This process is described by the Cahn–Hilliard equation [14,15], which is similar to the lubrication-type equation used to describe spinodal dewetting. The limiting dynamics are the "Ostwald ripening" process [20–24], which exhibits dynamic scaling as we see in our problem.

Recent experiments of coarsening dewetting films have been conducted by Limary and Green [25]. They measure dynamic scaling and find $N(t) \sim t^{-\beta}$, where β varies from about 0.1 to 0.4. Since their experiment is on a two-dimensional substrate, the one-dimensional results here cannot be quantitatively compared. However, they do find a crossover from diffusion-driven to coalescence dominated coarsening, which we explain here.

A review of the lubrication model and its reduction is given in Section 2. In Section 3, a local analysis of coarsening mechanisms is presented. Section 4 examines the global dynamics of coarsening, including scaling arguments for the statistical evolution and numerical results confirming our analysis.

2. The lubrication model

The dynamics of this physical system can be modeled by a lubrication equation for the evolution of the thickness of the fluid film coating the solid substrate, $h = h(x, t)$ [26–28]. In the limit of low Reynolds number, the Navier–

Stokes equations for the incompressible flow of a thin, slowly-varying film of viscous liquid take the form of a nondimensional Reynolds' equation,

$$\frac{\partial h}{\partial t} = \frac{\partial}{\partial x}\left(h^3 \frac{\partial p}{\partial x}\right),$$ (2.1)

where p defines the hydrodynamic pressure experienced by the film. The gradient of p gives the local forces on the fluid. For very thin films, the influence of gravity can be neglected and the dynamics are dominated by surface tension at the film's free surface and intermolecular forces at the fluid-substrate interface. A simple model for the pressure is then given by

$$p = \Pi(h) - \frac{\partial^2 h}{\partial x^2}.$$ (2.2)

The second term in (2.2) gives the linearized contribution of surface tension to the total pressure for a slowly-varying curved interface. The combined effects of all intermolecular forces between the solid substrate and a homogeneous film of thickness h is given by the disjoining pressure $\Pi(h)$, the derivative of the potential $U(h)$,

$$\Pi(h) \equiv \frac{\mathrm{d}U}{\mathrm{d}h}.$$ (2.3)

The total energy of the system is given in terms of contributions from this potential and the surface energy,

$$E = \int U(h) + \frac{1}{2}h_x^2 \, \mathrm{d}x.$$ (2.4)

We consider intermolecular potentials $U(h)$ including both attractive and repulsive effects, which balance to produce a single minimum at $h = \epsilon > 0$ [19]. This minimum corresponds to the nondimensional uniform film thickness which is globally-stable (see [27] for its dimensional meaning). Physically, it describes complete wetting of the solid substrate by at least a monolayer of the fluid. As will be discussed further, such "ultra-thin film" (UTF) or "pre-wetting" layers can have a dramatic influence on the dynamics of thin films since they regularize singularities associated with the motion of contact lines on dry solid substrates [26,29]. Much of the analysis is independent of the details of the potential $U(h)$, but for definiteness we suppose that it can be written as an ϵ-independent function $\mathcal{U}(H)$ with a minimum at $H = 1$ corresponding to the equilibrium UTF thickness,

$$U(h) = \mathcal{U}(h/\epsilon).$$ (2.5)

In this model, up to a critical thickness, all homogeneous thin films with $h = O(1)$ can be shown to be unstable [13,30,31]. Nearly-uniform films will break up and develop into sets of near-equilibrium droplets connected by UTF layers. Each fluid droplet is described by a localized steady-state solution of (2.1) and (2.2). These have been previously analyzed [13,19], and we briefly review them here. Nontrivial steady-state solutions of (2.1) and (2.2) have uniform, constant pressure, $p = \bar{p}$, where $\bar{p}$ is between 0 and the maximum of $\Pi(h)$, $p_{\max}$. That is, there is a continuous one-parameter family of droplet solutions, $h = \bar{h}(x; \bar{p})$, given by the homoclinic solution of

$$\frac{\mathrm{d}^2 \bar{h}}{\mathrm{d}x^2} = \Pi(\bar{h}) - \bar{p}.$$ (2.6)

For $|x| \to \infty$, the tails of droplet solutions approach the saddle point of (2.6) defining a modified UTF thickness determined by a balance of the disjoining pressure and $\bar{p}$, $\bar{h}(x) \to h_{\min}(\bar{p}) = \epsilon + O(\epsilon^2)$. In contrast, the disjoining pressure is relatively weak in the interior of the droplet, where $\bar{h} \gg O(\epsilon)$, and to leading order as $\epsilon \to 0$, the profile
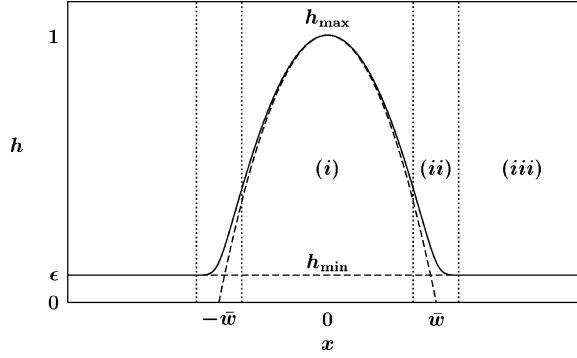
Fig. 2. A stable steady-state droplet solution $\bar{h}(x; \bar{p})$ showing the three regions in the asymptotic structure of the solution for $\epsilon \to 0$: (i) droplet core, (ii) contact line, (iii) outer ultra-thin film. The dashed curve shows the leading order asymptotic solution for the droplet core, the parabola (2.7), with width $2\bar{w}$.

is parabolic (Fig. 2), determined by a balance of surface tension and $\bar{p}$,

$$\bar{h}(x; \bar{p}) \sim \begin{cases} \frac{1}{2}\bar{p}(\bar{w}^2 - x^2) & |x| < \bar{w}, \\ h_{\min}(\bar{p}) & |x| > \bar{w}, \end{cases} \tag{2.7}$$

where $\bar{w} = \bar{w}(\bar{p})$ gives an effective measure of the (half-)width, or radius, of the droplet. The solutions $h = \bar{h}(x; \bar{p})$, parametrized by $\bar{p}$, constitute the one-parameter continuous family of steady state droplets, with mass inversely related to $\bar{p}$.

Since closed-form solutions cannot be found for all of the droplet properties for general $\Pi(h)$, it is helpful to compute leading order results by considering the limit of vanishing ultra-thin films, $\epsilon \to 0$. As described in [19], in this limit, the slope at the edge of droplet core, defining the contact angle, is given in terms of the intermolecular potential as $A = \sqrt{2|\mathcal{U}(1)|}$. To leading order, the width of the drop is then related to A by

$$\bar{w}(\bar{p}) \sim \frac{A}{\bar{p}}. \tag{2.8}$$

We can then define the mass of droplet as the mass of the core region,

$$\bar{m}(\bar{p}) \equiv \int_{-\bar{w}}^{\bar{w}} \bar{h}(x; \bar{p}) \, dx \sim \frac{2A^3}{3\bar{p}^2}. \tag{2.9}$$

Note that the size and mass of droplets are independent of ϵ and are determined by the droplet pressure $\bar{p}$.

2.1. Reduction to the droplet dynamical system

Non-identical droplets separated by finite distances are not steady states; however, such states are generally close to equilibrium and evolve slowly, on long timescales. Droplets of different sizes have different values of $\bar{p}$ and will be out of equilibrium due to mismatches in their surrounding UTF layers. It will be shown that their $h_{\min}$ values differ at $O(\epsilon^2)$. The quasi-steady dynamics of such droplets can be described in terms of the properties of the steady-state droplets. Fig. 3 shows a typical example of the interaction between droplets, showing two dynamical features: translation and mass exchange.

A derivation of the equations governing the droplet dynamics was obtained by studying the linearized stability of a single droplet [19]. The influences of neighboring droplets arise from the fluid fluxes J_-, J_+ (left and right,
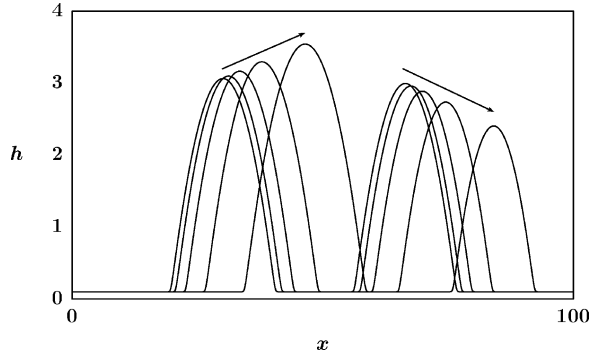
Fig. 3. Dynamics of two typical adjacent droplets in a dewetting film. The interaction of the droplets generally yields mass exchange and spatial motion.

respectively) which result from pressure gradients via

$$J \equiv -h^3 p_x. \tag{2.10}$$

The near-equilibrium form of the solution can then be written in terms of the steady-state droplet with slowly-varying parameters describing its position, $X(t)$, and its pressure $P(t)$, and perturbations on the order of the flux,

$$h(x, t) \sim \bar{h}(x - X(t); P(t)) + O(J). \tag{2.11}$$

The solvability conditions for this solution yield the evolution equations for $X(t)$, $P(t)$,

$$\frac{\mathrm{d}P}{\mathrm{d}t} = C_P(P)(J_+ - J_-), \qquad \frac{\mathrm{d}X}{\mathrm{d}t} = -C_X(P)(J_+ + J_-), \tag{2.12}$$

where C_P and C_X are coefficient functions which depend only on the equilibrium droplet shape:

$$C_X(P) = \frac{\int_{-\bar{w}}^{\bar{w}} ((\bar{h} - h_{\min})/\bar{h}^3) \, \mathrm{d}x}{2 \int_{-\bar{w}}^{\bar{w}} ((\bar{h} - h_{\min})^2/\bar{h}^3) \, \mathrm{d}x}, \tag{2.13}$$

and

$$C_P(P) = -\left(\int_{-\bar{w}}^{\bar{w}} \frac{\partial \bar{h}}{\partial \bar{p}} \, \mathrm{d}x \right)^{-1}. \tag{2.14}$$

The dynamics of a single droplet under (2.12) is given by combinations of the two basic modes of evolution: (i) translation with fixed mass (constant P) for $J_+ = J_-$, and (ii) change of mass at a fixed position (constant X) for $J_+ = -J_-$, see Fig. 4.

More generally, the governing equations for an array of N droplets, $\{X_k(t), P_k(t)\}$ for $k = 1, 2, \ldots, N$, are given by

$$\frac{\mathrm{d}P_k}{\mathrm{d}t} = C_P(P_k)(J_{k,k+1} - J_{k-1,k}), \qquad \frac{\mathrm{d}X_k}{\mathrm{d}t} = -C_X(P_k)(J_{k,k+1} + J_{k-1,k}), \tag{2.15}$$

where $J_{k,k+1}$ is the flux between droplets k and $k + 1$.

This reduction of the dynamics of the PDE (2.1) to coupled ODEs for the droplets is made possible by noting that the flux is nearly constant in the ultra-thin film layers between droplets [19]. As shown in [19], under appropriate conditions, the dynamics of the UTF between droplets is quasi-statically slaved to the evolution of the droplets. That is, (2.1) and (2.2) can be reduced to an elliptic problem for the "chemical potential" $\partial_{xx}[V(h)] = 0$, subject
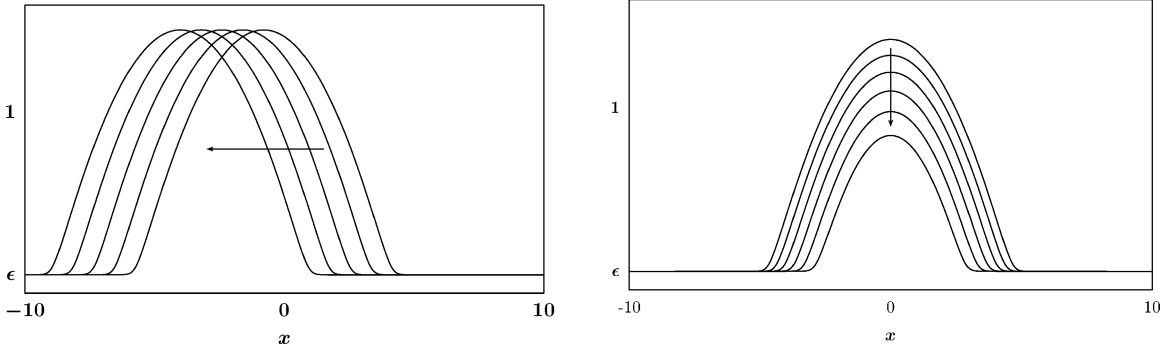
Fig. 4. Fundamental modes of evolution for a single droplet: (left) translation and (right) change of mass.

to the Dirichlet boundary conditions at the droplet edges, $V = V(h_{\min}(P_j))$ for $j = k, k + 1$. The function $V(h)$ is given explicitly in terms of the intermolecular potential as

$$V(h) = \int h^3 U''(h) \, dh. \tag{2.16}$$

Then the flux, $J \equiv -dV/dx$, since it is nearly constant in the UTF layers, can be approximated by

$$J_{k,k+1} = -\frac{V(h_{\min}(P_{k+1})) - V(h_{\min}(P_k))}{(X_{k+1} - \bar{w}(P_{k+1})) - (X_k + \bar{w}(P_k))}. \tag{2.17}$$

Eqs. (2.15) and (2.17) constitute a closed system of ODEs for the droplet pressures and positions.

2.2. The simplified dynamical model

The above derivation applies to a broad class of pressure potential functions $U(h)$. Once this function is specified, the details of the droplet solutions and the other functions in the model can be calculated. To make our study of this model more explicit, we will focus attention on a particular representative potential, $\mathcal{U}(H) = (H^{-3}/3) - (H^{-2}/2)$. This corresponds to the disjoining pressure,

$$\Pi(h) = \frac{\epsilon^2}{h^3} - \frac{\epsilon^3}{h^4}, \tag{2.18}$$

and yields $A = 1/\sqrt{3}$ in (2.8). This form of disjoining pressure was considered in [13,19,32]. Similar potentials with different powers for the repulsive term correspond to the standard 6-12 Lennard–Jones potential and other commonly used models [13,16,17,26,27,33]. The range of allowable pressures for homogeneous films covers $0 \leq \bar{p} \leq p_{\max} = 27/(256\epsilon)$. This range also covers the set of equilibrium droplets with $\bar{p} \to 0$ corresponding to very large drops and $\bar{p} \to p_{\max} = O(\epsilon^{-1})$ describing the smallest steady droplets distinguishable from the ultra-thin film.

From (2.14), we can obtain a good estimate of the pressure coefficient function as

$$C_P(P) \sim \frac{3}{4A^3} P^3. \tag{2.19}$$

Apart from the coefficient of P^3 in (2.19) and the condition defining the width (2.8), the leading order structure of droplets (2.7) is independent of the form of the disjoining pressure for $\epsilon \to 0$. However, the limit $\epsilon \to 0$ must be considered more carefully for other system properties. From (2.16), for (2.18) the corresponding monotone

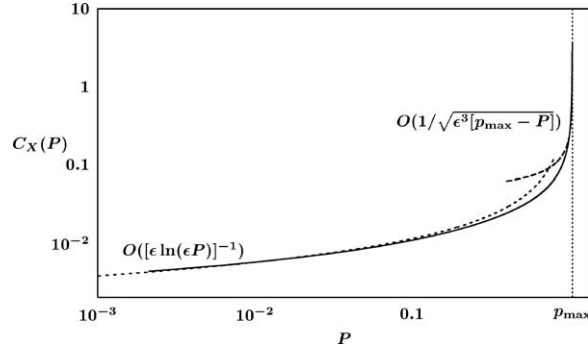Fig. 5. The $C_X(P)$ drift coefficient function (2.13) and its asymptotic behaviors for large drops ($P \to 0$) (2.22) and small drops ($P \to p_{max}$).

decreasing chemical potential is $V(h) = -\epsilon^2(4\epsilon/h + 3\ln h)$. From (2.6) the modified ultra-thin film thickness surrounding a drop is given by

$$h_{min}(\bar{p}) \sim \epsilon(1 + \epsilon\bar{p} + 4\epsilon^2\bar{p}^2). \qquad (2.20)$$

Combining these results, for $\epsilon \to 0$, we obtain $V(h_{min}(\bar{p})) \sim -\epsilon^2(4 + 3\ln\epsilon) + \epsilon^3\bar{p}$, consequently, the inter-droplet flux (2.17) reduces to

$$J_{k,k+1} \sim \frac{-\epsilon^3(P_{k+1} - P_k)}{X_{k+1} - (A/P_{k+1}) - X_k - (A/P_k)}. \qquad (2.21)$$

Finally, the calculation of the drift coefficient (2.13) is more involved (see Appendix A), but it can be shown that except for very small droplets, this function can be approximated by

$$C_X(P) \sim \frac{B}{\epsilon \ln(P/p_{max})} > 0, \qquad (2.22)$$

where B is a negative constant, independent of ϵ, see Fig. 5.

In the following sections we will use these estimates to rescale and simplify the droplet system (2.15). First we describe the mechanisms of coarsening, a key element of the dynamics of droplets in the original PDE that must be added to the droplet ODE system.

3. Mechanisms for coarsening

The system of ODEs (2.15) describing the evolution of droplet arrays was derived for near-equilibrium states, where the dynamics occur on slow time-scales. This is the case when all of the drops have finite masses and are well-separated, and consequently all of the fluxes are uniformly small, $O(\epsilon^3)$.

There are two situations where the fluxes become large and the validity of the ODEs breaks down:

(i) *Droplet collapse*: The flux between two drops can become large if one drop's pressure becomes large. Equilibrium droplets have mass decreasing with increasing pressure, see (2.9), up to $P \leq p_{max} = O(\epsilon^{-1})$. A droplet that is shrinking (see Fig. 4b) has $P_k(t) \nearrow p_{max}$ as it starts to "melt" into the surrounding ultra-thin film and eventually disappears. As this occurs, the flux briefly becomes large, $J = O(\epsilon^2) \gg O(\epsilon^3)$. We identify that a droplet collapse event is occurring if any drop satisfies the *collapse condition*:

$$P_k(t) \geq (1 - \mu)p_{max}, \qquad (3.1)$$

where $\mu > 0$ is a small parameter.

(ii) *Droplet collision*: If two droplets approach each other then the denominator of the flux between them (2.17) goes to zero and hence the local flux becomes large; thereafter the two drops will rapidly merge together. We identify that a droplet collision event is occurring if the adjacent contact lines of any pair of drops satisfy the *collision condition*:

$$|(X_{k+1} - \bar{w}(P_{k+1})) - (X_k + \bar{w}(P_k))| \le \delta, \tag{3.2}$$

where $\delta = O(\epsilon) > 0$ is a small parameter.

In both of these scenarios, the break down of the validity of (2.15) coincides with a *coarsening event*, where the number of drops in the system decreases by one. The details of such coarsening events is a behavior of the original PDE ((2.1) and (2.2)) that is not captured by the slow-time reduced model (2.15). Having a large local flux means that the coarsening events evolve on a much faster timescale. We will treat these events as occurring instantaneously relative to the $O(\epsilon^{-3})$ timescale of (2.15). Consequently, when one of the coarsening condition (3.1) or (3.2), is detected in a simulation for N drops, the solution of (2.15) is halted, a modification to the set of drops is made to account for the effect of the coarsening event and then the ODE system (2.15) is restarted to describe the further evolution of the remaining $N - 1$ drops.

This type of piecewise continuous dynamical system on a decreasing set of interacting elements has been called a coarsening dynamical system [34]. The complete description of the dynamical system is given by the ODEs (2.15), the coarsening event detection conditions (3.1) and (3.2), and rules (sometimes called extinction or *coarsening rules* [35]) for how the set of N drops is reduced to a set of $N - 1$ drops by each coarsening event.

We now consider the description of the coarsening rules based on the behavior of the ODE system leading up to the coarsening event and the dynamics of the full PDE for the far-from-equilibrium behavior at the instant of the coarsening event.

3.1. Single-droplet collapse

We begin by briefly reviewing the description of droplet collapse given in [19] and expanding on the analysis. Suppose that drop k is initially smaller than both of its neighbors, $P_k(0) > P_{k-1}(0)$ and $P_k(0) > P_{k+1}(0)$. From (2.21), the fluxes set-up by these pressures will both serve to further increase $P_k(t)$. If the drops are widely separated, then we can neglect the influence of droplet motion on the evolution of the pressure. Consequently, using (2.19) and (2.21) to reduce (2.15) to its dominant term for the evolution of $P_k(t)$ yields

$$\frac{\mathrm{d}P_k}{\mathrm{d}t} \propto \epsilon^3 P_k^4, \tag{3.3}$$

with a weak dependence on the pressures of the neighboring drops. This equation yields finite-time blow-up of the pressure $P_k(t) = O((t_c - t)^{-1/3}) \to \infty$ as $t \to t_c$. As this proceeds, the drop's mass and width steadily decrease, $M_k \sim O((t_c - t)^{2/3}) \to 0$, $\bar{w} \sim O((t_c - t)^{1/3}) \to 0$. In reality, this blow-up cannot occur as the pressure is bounded by $p_{\max}$, but it does mean that the drop will satisfy the collapse condition (3.1) at a finite time, $t_\mu < t_c$. When this takes place, the drop has effectively vanished into the UTF. Thereafter drop k is removed from the set of drops, its neighbors, drops $k - 1$ and $k + 1$, are re-assigned to be adjacent drops, and the evolution of the remaining $N - 1$ drops can be resumed with (2.15); this is the coarsening rule for collapse. The collapse of a drop necessarily influences the other drops in the system through the coupled fluxes and conservation of mass. However, as suggested by model (3.3), the influence of the rest of the system on the collapsing drop is weak.

Collapse is a coarsening mechanism involving individual drops "dying alone". In contrast, the description of collisions is more complicated.
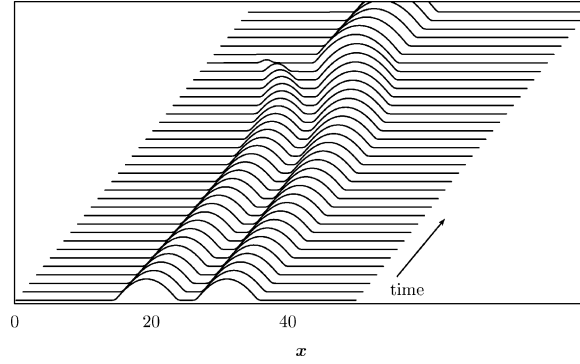
Fig. 6. Numerical simulation of two interacting drops in the lubrication PDE (2.1). As predicted by the ODE model (3.4), collision cannot occur.

3.2. Analysis of two-droplet interactions: no collisions

We show that the two-droplet collision process is necessarily non-local; that is, two droplets cannot collide without the influence of external fluxes provided by neighboring droplets. The need for these fluxes is made clear by considering the dynamics of two droplets without any external forcing. In this case, the governing system of ODEs (2.15) takes the form

$$\frac{\mathrm{d}X_1}{\mathrm{d}t} = -C_X(P_1)J_{1,2}, \qquad \frac{\mathrm{d}X_2}{\mathrm{d}t} = -C_X(P_2)J_{1,2}. \tag{3.4a}$$

$$\frac{dP_1}{dt} = C_P(P_1)J_{1,2}, \qquad \frac{dP_2}{dt} = -C_P(P_2)J_{1,2}. \tag{3.4b}$$

In the special case of two droplets of equal size, the flux vanishes due to symmetry ($J_{1,2} = 0$) and no droplet motion occurs (in the PDE, motion will occur on exponentially slow timescales).

Consider two quasi-stable drops, initially described by $\{X_1(0), P_1(0)\}$ and $\{X_2(0), P_2(0)\}$ with $X_1(0) < X_2(0)$. Without loss of generality, suppose that the first drop is smaller than the second, so that $P_1(0) > P_2(0)$. From (2.21), the flux between them, $J_{1,2} \propto -\epsilon^3(P_2 - P_1)$ is initially positive. Since the $C_P(P)$ coefficient function (2.19) is a positive increasing function, from (3.4b) we see that $P_1(t)$ is increasing (and the first drop gets steadily smaller) while $P_2(t)$ is decreasing (and the second drop gets steadily larger). The $C_X(P)$ coefficient function is a positive increasing function (2.22), and from (3.4a) we see that both drops will move to the left, $X_1(t)$ and $X_2(t)$ are both decreasing. Since $P_1(t) > P_2(t)$ the speed of the first drop is always larger than that of the second, hence the separation between the droplets will steadily increase. Consequently, collisions cannot occur with only two drops, see Fig. 6.

3.3. Collisions

We now focus attention on the spatial interactions that lead to collision events. Whereas (3.3) is a simplified model of (2.15) focusing on the evolution of droplet pressures and neglecting their motions, we now consider the opposite extreme. That is, assume the system is in a regime where the droplet pressures change slowly compared to the droplet positions. This implies that the possibility of collapse events is neglected in favor of the dominant role of collision interactions. The system conditions defining this regime will be describing in more detail in Section 4.

To study how collisions can occur, consider a system of four drops: a pair that will collide (drops 2 and 3) and their nearest neighbors (drops 1 and 4), see Fig. 7. Define the distance separating the contact lines of neighboring drops as

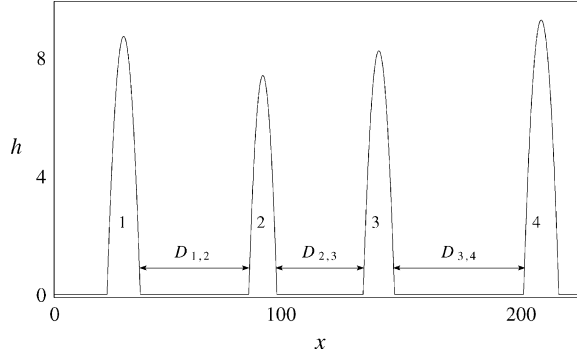$$D_{k,k+1} \equiv (X_{k+1} - \bar{w}(P_{k+1})) - (X_k + \bar{w}(P_k)). \tag{3.5}$$

Fig. 7. A schematic figure of a system of four drops used to study collision interactions.

Clearly all of the D's are initially positive and in this notation the collision condition (3.2) is that $D_{k,k+1} \leq \delta$ for some pair of drops.

Assuming that the pressures are all $O(1)$ and evolve slowly in time, they will have a negligible influence on the evolution of the D's. Then the evolution equations for the $D_{k,k+1}$'s can be obtained from the evolution equations for the X_k's (2.15),

$$\frac{\mathrm{d}D_{1,2}}{\mathrm{d}t} = \frac{\beta_{1,2} - \alpha_{1,2}}{D_{1,2}} + \frac{\alpha_{2,3}}{D_{2,3}} \tag{3.6a}$$

$$\frac{\mathrm{d}D_{2,3}}{\mathrm{d}t} = -\frac{\beta_{1,2}}{D_{1,2}} + \frac{\beta_{2,3} - \alpha_{2,3}}{D_{2,3}} + \frac{\alpha_{3,4}}{D_{3,4}} \tag{3.6b}$$

$$\frac{\mathrm{d}D_{3,4}}{\mathrm{d}t} = -\frac{\beta_{2,3}}{D_{2,3}} + \frac{\beta_{3,4} - \alpha_{3,4}}{D_{3,4}}, \tag{3.6c}$$

where the numerators on the right-hand side are given by pressure-dependent parameters

$$\alpha_{k,k+1} = \epsilon^3 C_X(P_k)(P_{k+1} - P_k), \qquad \beta_{k,k+1} = \epsilon^3 C_X(P_{k+1})(P_{k+1} - P_k). \tag{3.7}$$

Since $C_X(P)$ is positive, these parameters are positive or negative together according to the sign of $(P_{k+1} - P_k)$.

Careful examination of the form of system (3.6) allows us to determine how collision of drops 2 and 3 can occur in finite time, that is $D_{2,3} \to 0$ as $t \to t_c$. First, consider the simplest possibility, where the influence of the neighboring drops is negligible. Then the leading order dynamics for (3.6b) as $t \to t_c$ are given by

$$\frac{\mathrm{d}D_{2,3}}{\mathrm{d}t} \sim \frac{\beta_{2,3} - \alpha_{2,3}}{D_{2,3}} \to D_{2,3} \sim O(\sqrt{2(\alpha_{2,3} - \beta_{2,3})(t_c - t)}). \tag{3.8}$$

A physically acceptable solution (i.e. with $D_{2,3}$ real-valued) requires that $\alpha_{2,3} > \beta_{2,3}$. But since $C_X(P)$ is a positive increasing function of the pressure, for all values of P_k, P_{k+1}, we get

$$\beta_{k,k+1} - \alpha_{k,k+1} = \epsilon^3 (C_X(P_{k+1}) - C_X(P_k))(P_{k+1} - P_k) \geq 0; \tag{3.9}$$

hence (3.8) cannot be the case. This is consistent with the result from the previous section, where we showed that two drops cannot collide without external influences.

While "isolated collision" cannot occur, we now show that the mutual coupling of two pairwise interactions can generate collisions. Consider an interaction of drops 1–3, with drop 4 having a weak influence on the dynamics.

Then (3.6) reduces to the phase plane system,

$$\frac{dD_{1,2}}{dt} = \frac{\beta_{1,2} - \alpha_{1,2}}{D_{1,2}} + \frac{\alpha_{2,3}}{D_{2,3}} \qquad \frac{dD_{2,3}}{dt} = -\frac{\beta_{1,2}}{D_{1,2}} + \frac{\beta_{2,3} - \alpha_{2,3}}{D_{2,3}}. \tag{3.10}$$

It can be shown that in order for $D_{2,3} \to 0$ in finite time $D_{1,2}$ must also go to zero and $\beta_{1,2}$ must be positive. Such a pairwise collision $\{D_{1,2}, D_{2,3}\} \to 0$, also requires that $\alpha_{2,3} < 0$. Then from (3.7), we find that $P_2 > P_1$ and $P_2 > P_3$. That is, collision can occur when two larger drops are attracted toward a smaller drop between them, see Fig. 7. A similar three-element "pinch" collision scenario was described between kinks and anti-kinks in a Cahn–Hilliard equation in [34].

Similarly, if $\beta_{1,2} < 0$ then $D_{2,3} \to 0$ requires that $\alpha_{3,4} < 0$. Further, for $D_{3,4} \to 0$, $\beta_{2,3}$ must be positive. Consequently, drops 2–4 can collide if their pressures satisfy $P_2 < P_3$, $P_3 > P_4$. This could be expected from the spatial invariance of the problem.

This ODE argument suggests that collision events involving three drops merging into one should be commonly seen in numerical simulations of the lubrication PDE (2.1). Actually, only two-drop collisions are generically seen in the PDE, see Figs. 1 and 10. To reconcile these observations it is crucial to incorporate the influence of the collision condition (3.2) in interpreting of the results from the ODE model (2.15). Consider the case where drops 1, 2, and 3 collide as described by (3.10). To leading order as $t \to t_c$, the solution of this system takes the form

$$D_{1,2}(t) \sim \rho_{1,2}\sqrt{t_c - t}, \qquad D_{2,3}(t) \sim \rho_{2,3}\sqrt{t_c - t}, \tag{3.11}$$

where $\rho_{1,2}$ and $\rho_{2,3}$ are positive constants. As $t \to t_c$, the ratio of $D_{2,3}$, $D_{1,2}$ approaches a constant,

$$r = \frac{D_{2,3}}{D_{1,2}}, \tag{3.12}$$

which can be obtained from (3.10) as the positive solution of the quadratic equation

$$(\beta_{1,2} - \alpha_{1,2})r^2 + (\alpha_{2,3} + \beta_{2,3})r - (\beta_{2,3} - \alpha_{2,3}) = 0. \tag{3.13}$$

This ratio is a function of the three droplet pressures, $r = r(P_1, P_2, P_3)$ and is positive if P_1 and P_3 are both less than P_2 (as was found necessary for collisions above). Fig. 8 shows a plot of the contour lines of r.

Solutions (3.11) are defined for $t \leq t_c$, however, the collision condition (3.2) enforces a cut-off on the evolution at an earlier time $t_\delta < t_c$, when one of the separation distances satisfies $D(t_\delta) = \delta$. Which pair of drops, 1 and 2 or 2 and 3, satisfy this condition at t_δ depends on the ratio r; if $r > 1$ then drops 1 and 2 collide, if $r < 1$ then drops 2 and 3 collide, $r = 1$ is the degenerate symmetric case when both pairs collide. From Fig. 8, we see that the case
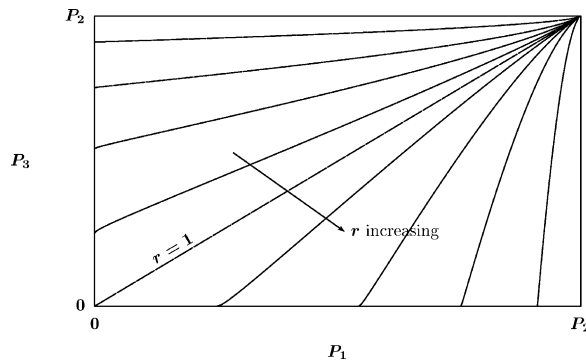

Fig. 8. Contour lines of the asymptotic collision distance ratio, $r = D_{2,3}/D_{1,2}$ (3.12), as a function of P_1, P_3 for a fixed value of P_2. This structure of the solution is generic for all values of P_2.
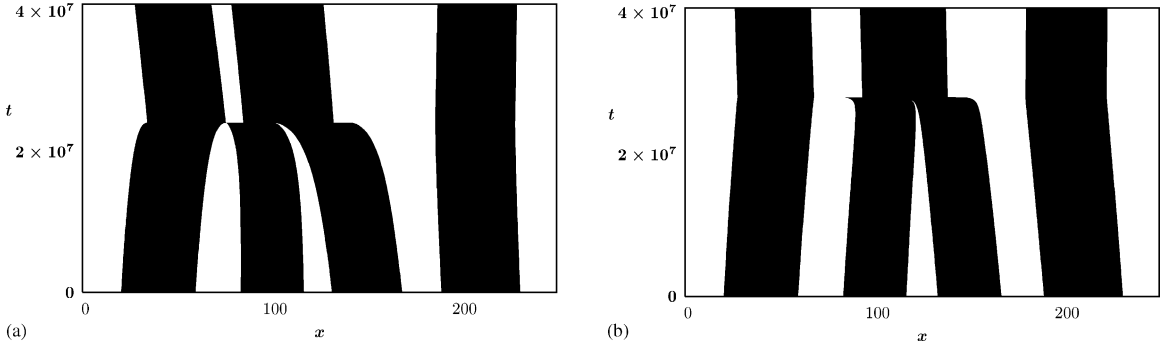
Fig. 9. Plots of droplet histories in the xt plane for two different versions of the collision events suggested by (3.6): (a) a nearly symmetric 3-drop interaction, and (b) a more asymmetric quasi-2-drop collision. The solid stripes indicate the positions of droplet cores, with supports given on $|x - X_k(t)| \leq \bar{w}(P_k)$ for $k = 1, 2, 3, 4$.

$r > 1$ occurs if $P_1 > P_3$ and conversely $r < 1$ if $P_3 > P_1$, therefore, we conclude that droplet 2 will collide with the *smaller* of its two neighboring drops. Fig. 9 shows droplet path-histories for two typical collision events for the solution of (2.15) starting with initial conditions for four drops with the general form shown in Fig. 7. The two simulations are identical except for a 10% change in the mass of drop 3. In both cases drops 2 and 3 collide so $r < 1$, however, we note the influence of the value of r on the qualitative form of the collision:

- In Fig. 9a, where r is near one, the two pairs of drops come together in a nearly-symmetric "*3-drop pinch*."
- In Fig. 9b, where $r \ll 1$, there is a large degree of asymmetry between the droplet pairs. Indeed, it appears as if droplet 1 has a relatively weak interaction with drops 2 and 3, yielding a "*quasi-2-drop collision*."

The qualitative character of the collision will also depend on droplet positions in as far as it will affect how closely the asymptotic regime (3.12) is approached in (3.10) before the collision condition applies. Fig. 10 shows the details of the coarsening events from Fig. 1 obtained from the numerical solution of the original lubrication PDE. We observe a collision event at $t \approx 660,000$ that is very similar to the collisions described by the ODE system in Fig. 9. The other coarsening event, at $t \approx 500,000$, is a droplet collapse. It is interesting to note that this event also has a similar structure: two larger droplets approach a smaller middle droplet in a more-or-less symmetric manner. Hence, in general there can be a competition between collision and collapse as a mechanism for coarsening, and which will dominate may not be immediately obvious from the qualitative form of the initial data. This will be explored more fully in Section 4.

A question of interest is whether four-drop collisions are also possible in (3.6). That is, can the mutual interaction of $D_{1,2}$, $D_{2,3}$, $D_{3,4}$ force all three to zero in finite time? In (3.6a), we need $\alpha_{2,3} < 0$ to drive collision. In (3.6c), we need $\beta_{2,3} > 0$; however, from (3.7) these two conditions yield a contradiction for the relation between P_2 and P_3. Consequently, four-drop collisions cannot take place and only the scenarios described above can occur.

It is important to note that once one pair of drops has collided in (3.11), the further dynamics will be radically altered. In particular, unless we are in the exactly symmetric case of $r = 1$, the other pairwise collision will not take place, as seen in Figs. 9 and 10. How the dynamics proceed after the collision at t_δ is examined next.

3.4. The coarsening rule for collisions: merging

The ODE models described above give the near-equilibrium evolution leading up to a collision event (3.2) at time t_δ. At that point, the local solution is far from equilibrium, and analysis of PDE ((2.1) and (2.2)) is needed to describe the ensuing droplet merging process.
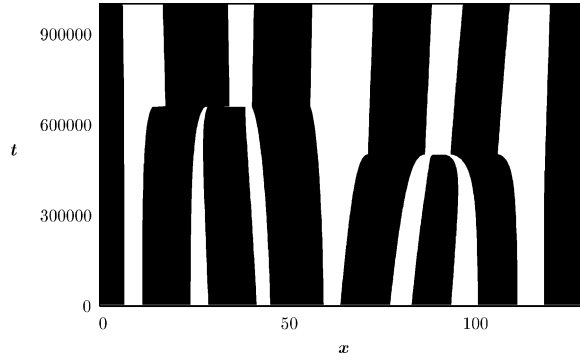
Fig. 10. Droplet histories in the *xt* plane (corresponding to Fig. 1) from numerical simulations of the full PDE, notice that the collision event (left) resembles the asymmetric "quasi-2-drop" collision in Fig. 9b, while the collapse event (right) is more symmetric.

Fig. 11 shows details of the stages of evolution involved in the collision event from the simulation shown in Fig. 1. The first frame shows slow evolution that is well-described by (2.15) until the adjacent edges of the drops get sufficiently close. Then the evolution becomes much more rapid as the two drops merge together to briefly form a convex "two-droplet complex" which reduces the surface energy of the system, relative to that of the two adjacent equilibrium drops. This transient structure is unstable and rapidly equilibrates to yield a single droplet.
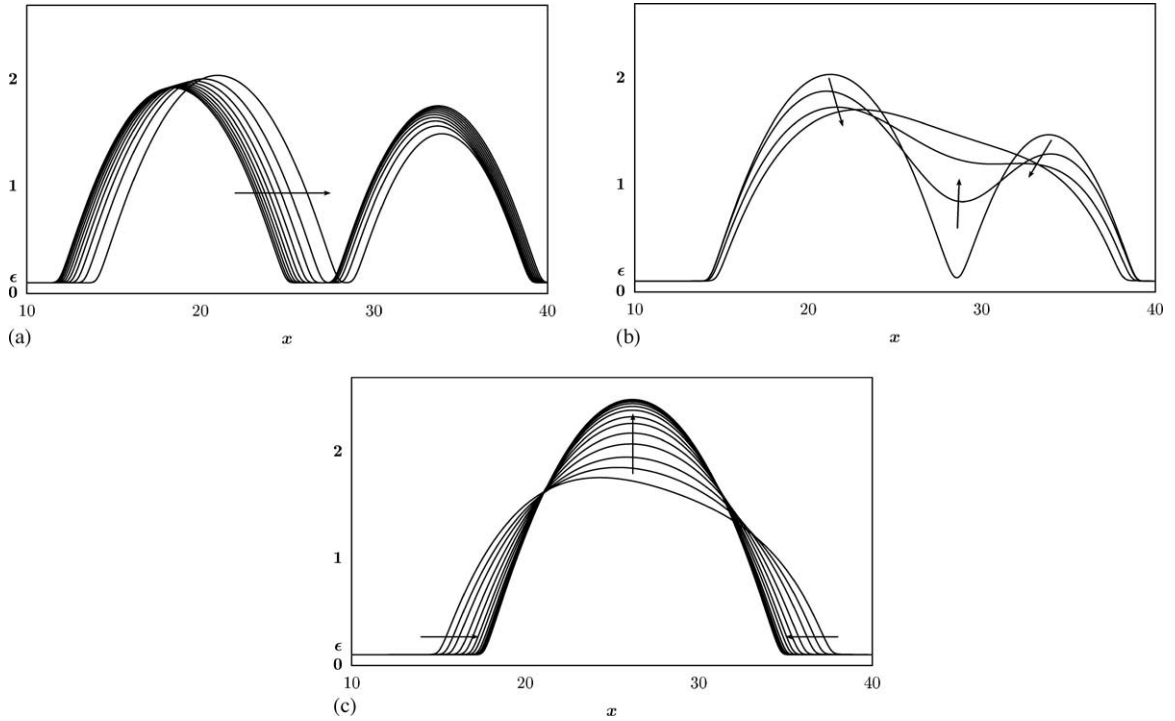

Fig. 11. Details of the collision and merging process: (a) two near-equilibrium droplet evolving toward collision, (b) the formation of the collided "two-drop complex" and its rapid convexification, (c) symmetrization and contraction to yield a single merged near-equilibrium droplet.

Getting the precise details of this merging process would generally require numerical solutions of the PDE, but a lot of insight into the expected behavior can be obtained without computations. The problem has conservation of mass, hence the mass of the merged drop, $m_{k,k+1}$, should be given by the total of the masses of the two drops, $m_{k,k+1} = m_k + m_{k+1}$. Therefore (2.9) yields a relation between the pressures before and after the collision,

$$P_{k,k+1} = \left(\frac{1}{P_k^2} + \frac{1}{P_{k+1}^2} \right)^{-1/2}. \tag{3.14}$$

It is less straightforward to obtain the position of the merged drop, $X_{k,k+1}$, since there is no exact conservation law for the center of mass. However, this position can be estimated using the analysis of the dynamics of a general convex drop relaxing to an equilibrium droplet profile done by one of the authors [32]. There it was found that the motion of the droplet edges (or contact lines) was much slower than the dynamics within the merged droplet core. In Fig. 11, we observe that the solution becomes convex before there is significant motion of the outer contact lines. The final stage is the convergence to the parabolic droplet profile (2.7). Given this description of the merging process, we can model the position of the merged droplet as being approximately symmetric with respect to the outer contact lines of the two colliding drops,

$$X_{k,k+1} = \tfrac{1}{2}[X_k - \bar{w}(P_k) + X_{k+1} + \bar{w}(P_{k+1})]. \tag{3.15}$$

Together, Eqs. (3.14) and (3.15) relate the state of the droplets just before collision, t_δ^-, to the properties of the merged droplet just after the collision, t_δ^+. By mapping the merged state onto one of the two drops involved in the collision $\{P_{k,k+1}, X_{k,k+1}\} \to \{P_k, X_k\}$, and eliminating the other, we obtain a reduced system of $N-1$ drops governed by (2.15) for $t > t_\delta$.

In summary, the coarsening rules given here and in Section 3.1 prescribe how the droplet dynamical system (2.15) must be modified to avoid the break-downs in validity signaled by the coarsening conditions (3.1) and (3.2). This augmented coarsening dynamical system gives a model for the evolution of the droplets for all times, until the final one-drop stable steady state is reached. For the remainder of this article, we will examine the larger-scale implications of the two coarsening mechanisms.

3.5. Energy considerations

The energy of the system (2.4) is dissipated as a generalized gradient flow with the rate of dissipation

$$\frac{\mathrm{d}E}{\mathrm{d}t} = -\int h^3 p_x^2 \, \mathrm{d}x \leq 0. \tag{3.16}$$

The contributions to the total energy from droplets are positive and dominated by the surface gradients. For the ultra-thin film, the energy is dominated by the potential and is negative, $U(h_{\min}) \sim U(\epsilon) < 0$. A consequence is that the energy is decreased whenever the fraction of the domain covered by the ultra-thin film is increased; this favors coarsening.

Both mechanisms for coarsening lead to a decrease in the fraction of the domain containing droplets. For a collapse event, the net change to the system is the loss of a single droplet and the gain of additional UTF of equal area,

$$\Delta E_{\text{collapse}}(P_k) \approx -\tfrac{1}{3} P_k^2 \bar{w}^3(P_k) + 2U(\epsilon)\bar{w}(P_k) < 0. \tag{3.17}$$

For a collision, the net change to the system involves replacing two drops with one merged drop and an accompanying gain of some UTF freed-up by the consolidation,

$$\begin{aligned}
\Delta E_{\text{collision}}(P_k, P_{k+1}) \approx &-\tfrac{1}{3}(P_k^2 \bar{w}^3(P_k) + P_{k+1}^2 \bar{w}^3(P_{k+1}) - P_{k,k+1}^2 \bar{w}^3(P_{k,k+1})) \\
&+ 2U(\epsilon)(\bar{w}(P_k) + \bar{w}(P_{k+1}) - \bar{w}(P_{k,k+1})) < 0.
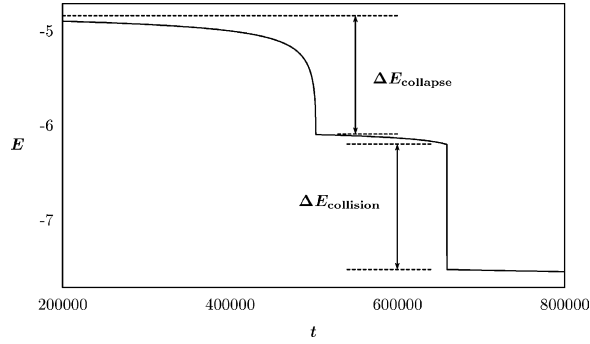\end{aligned} \tag{3.18}$$

Fig. 12. Evolution of the energy for the numerical solution of the PDE, corresponding to the dynamics shown in Figs. 1 and 10 including a collision and a collapse event.

In both cases, both the decrease in the number of drops and the increase in UTF area decrease the total energy. However, there is a qualitative difference between the energetics of these events. In a collapse, the decrease of energy occurs via a smooth and continuous near-equilibrium process, as described by (3.3) with $\Delta E_{\text{collapse}} \sim -O((t_c - t)^{-1/3})$ for $t \to t_\mu \lesssim t_c$. In contrast, on the timescale of the coarsening dynamics, the change in energy for collisions happens nearly instantaneously, as described in the previous section. The evolution of the energy for the original PDE ((2.1) and (2.2)) must be continuous for all times (see Fig. 12). But, a consequence of this rapid decrease in energy for the PDE when collisions occur is that the energy for the ODE coarsening model (2.15) will include jumps of size $\Delta E_{\text{collision}}$ at collision times t_δ.

As a result, coarsening events and their types can be identified from the evolution of the energy (2.4). We will see that energetics are not sufficient to predict the dynamics of coarsening in the system, but scaling analysis can provide insight on the behavior of large arrays of droplets.

4. Coarsening dynamics: collapse versus collision

Instabilities of thin films on large domains lead to the formation of large numbers of droplets upon dewetting. To describe the global behavior of such systems, we must understand the nature of the long term coarsening process. It is important to analyze how both of the coarsening mechanisms are influenced by the global properties of the system.

In particular, we consider a problem starting with a total fluid mass M, on a domain of length L, containing N drops. This state can result from the dewetting of a homogeneous film with thickness $H_c = M/L$. We define characteristic length and mass scales for typical drops in this system as

$$L_c = \frac{L}{N}, \qquad M_c = \frac{M}{N}. \tag{4.1}$$

Using (2.9), we can obtain a characteristic drop pressure in terms of the characteristic mass,

$$P_c = \sqrt{\frac{2A^3}{3M_c}}. \tag{4.2}$$

These scales will be used to obtain a reduced model from (2.15) and identify the parameters that control the balance between collision- and collapse-controlled coarsening.

4.1. The rescaled system for the dilute limit

We begin by assuming that the drops are spaced far enough apart, so that their widths are negligible, $\bar{w}(P_c) \ll L_c$. We call this the *dilute limit*. In the "dense" case, when this assumption is not true, the drops may be far from equilibrium as condition (3.2) may apply, with many collisions occurring in rapid succession. For near-equilibrium droplet arrays in the dilute limit, we may approximate the flux by the simpler expression,

$$J_{k,k+1} = -\epsilon^3 \frac{P_{k+1} - P_k}{X_{k+1} - X_k}. \tag{4.3}$$

Using (4.1) and (4.2), we rescale the pressures and positions for the N droplets $k = 1, 2, \ldots, N$, and the time as

$$P_k(t) = P_c \mathcal{P}_k(\tau), \qquad X_k(t) = L_c \mathcal{X}_k(\tau), \qquad t = \frac{4A^3 L_c}{3\epsilon^3 P_c^3} \tau, \tag{4.4}$$

and using (2.19), (2.22), and (4.3), system (2.15) becomes

$$\frac{d\mathcal{P}_k}{d\tau} = -\mathcal{P}_k^3 \left(\frac{\mathcal{P}_{k+1} - \mathcal{P}_k}{\mathcal{X}_{k+1} - \mathcal{X}_k} - \frac{\mathcal{P}_k - \mathcal{P}_{k-1}}{\mathcal{X}_k - \mathcal{X}_{k-1}} \right), \tag{4.5a}$$

$$\frac{d\mathcal{X}_k}{d\tau} = -\frac{\mathbb{K}}{\ln(\mathbb{R}\mathcal{P}_k)} \left(\frac{\mathcal{P}_{k+1} - \mathcal{P}_k}{\mathcal{X}_{k+1} - \mathcal{X}_k} + \frac{\mathcal{P}_k - \mathcal{P}_{k-1}}{\mathcal{X}_k - \mathcal{X}_{k-1}} \right). \tag{4.5b}$$

The two control parameters in the system are

$$\mathbb{K} = -\frac{4A^3 B}{3\epsilon P_c^2 L_c} > 0, \qquad \mathbb{R} = \frac{P_c}{p_{max}} < 1, \tag{4.6}$$

where the constant B comes from (2.22).

Using (2.9) one can show that

$$\mathbb{K} = O\left(\frac{H_c}{\epsilon} \right). \tag{4.7}$$

In other words, the "coarsening number" $\mathbb{K}$ is proportional to the ratio of the mean film thickness H_c to the UTF scale ϵ. Since mass is conserved, $\mathbb{K}$ is independent of time; in particular, it does not depend on the number of droplets in the system, $N(t)$. Because it appears as a prefactor in (4.5b), $\mathbb{K}$ measures the relative importance of drift to mass-exchange effects. Therefore dewetting of a relatively thin layer of fluid will lead primarily to mass-exchange dynamics, whereas a thick film will evolve into droplets controlled primarily by the drift mechanism.

The other scaling parameter, $\mathbb{R}$, is a ratio of typical droplet pressure to the reference pressure of vanishingly small equilibrium drops $p_{max} = O(\epsilon^{-1})$. Since P_c depends on the number of droplets ($P_c = O(\sqrt{N})$), $\mathbb{R}$ does change throughout the coarsening process. However, its effects on the overall dynamics are weak, because of the logarithmic dependence in (4.5b). More is said about this point in Section 4.3.

Our interest is in how the form of (4.5) affects the nature of the coarsening process, that is, how the number of drops decreases with time. From (4.1) and (4.2) we see that the characteristic scales L_c, P_c depend on time through $N(t)$. However, we note that $N(t)$ is constant over each time-interval when (4.5) applies and decreases by one for each coarsening event described in Section 3. Therefore, for systems with large numbers of drops, the influence of coarsening on (4.5) is a change in the characteristic scales which is slowly-varying compared to the droplet dynamics when $N \gg 1$.

4.2. Global instabilities and the onset of coarsening

In Section 3, we examined coarsening events as isolated local occurrences in systems (this is sometimes called nucleation [36]). Another useful point of view is the use of linearized analysis to study global instabilities which may lead to coarsening [34]. Here we will identify the fastest growing modes of (4.5) and connect them with coarsening by collision or collapse.

Formally, any array of drops of uniform size, $\mathcal{P}_k = 1$, with any set of positions $\mathcal{X}_k$ is an equilibrium of (4.5). These states are meta-stable and evolve according to exponentially slow dynamics [37] not described in this model. Consider the linearized evolution of perturbations to these states. For simplicity, let the base solution be a set of identical, equally-spaced drops with $\bar{\mathcal{P}}_k = 1$ and $\bar{\mathcal{X}}_{k+1} - \bar{\mathcal{X}}_k = 1$. Let the perturbed solutions be $\mathcal{P}_k(\tau) = \bar{\mathcal{P}}_k + \varepsilon \hat{P}_k(\tau)$, $\mathcal{X}_k(\tau) = \bar{\mathcal{X}}_k + \varepsilon \hat{X}_k(\tau)$. Linearizing (4.5) about the base state for $\varepsilon \to 0$ yields

$$\frac{d\hat{P}_k}{d\tau} = -(\hat{P}_{k+1} - 2\hat{P}_k + \hat{P}_{k-1}), \tag{4.8a}$$

$$\frac{d\hat{X}_k}{d\tau} = -\frac{\mathbb{K}}{\ln \mathbb{R}}(\hat{P}_{k+1} - \hat{P}_{k-1}). \tag{4.8b}$$

Note that the equation for the pressure perturbations is decoupled from (4.8b) and can be solved in the form

$$\hat{P}_k(\tau) = e^{ik\sigma}e^{\lambda\tau}, \qquad \lambda(\sigma) = 2 - 2\cos\sigma. \tag{4.9}$$

All of the eigenvalues are non-negative and lie in the range $0 \le \lambda \le 4$, hence this is a strongly unstable state. This could be expected since (4.8a) describes a spatial discretization of an ill-posed backward heat equation of the form $\partial_t \hat{P} = -\partial_{zz}\hat{P}$ [38]. For a system of N drops, the most unstable mode has $\sigma \approx \pi/(2N)$ with

$$\hat{P}_k(\tau) \approx (-1)^k e^{4\tau}. \tag{4.10}$$

That is, alternating drops will grow/shrink, see Fig. 13a. From (4.8b), we note that there is no relative motion between drops for this linearized mode, i.e. $\hat{X}_k = 0$, since $\hat{P}_{k+1} = \hat{P}_{k-1}$.

This instability mode can be expected to lead to coarsening by collapse. It sets up the conditions needed for collapse described in Section 3.1, every other droplet is surrounded by larger neighbors. However, as described in Section 3.3, these are also the conditions required for collisions. Further considerations are needed to determine which mode of coarsening will really occur.

If $|\mathbb{K}/\ln(\mathbb{R})| \ll 1$ then the time-scale for all modes of spatial motion will be slow compared to the evolution of the pressure perturbations. In this case, then spatial motion of the drops is largely negligible and collapse will indeed be the dominant mode of coarsening.
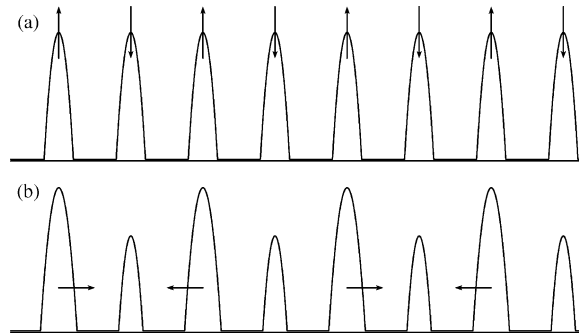

Fig. 13. Schematic of the fastest growing global instability modes: (a) the primary instability, connected to coarsening by collapse (4.10), and (b) the dominant secondary instability, connected to coarsening by collision (4.13).

On the other hand, if $|\mathbb{K}/\ln(\mathbb{R})| \gg 1$ then droplet motion can become dominant away from the base equilibrium state described above. In this case, the evolution of the pressures will occur slowly compared to changes in $\mathcal{X}_k(\tau)$, and we can neglect the evolution of the $\mathcal{P}_k$'s for the purpose of linear stability analysis. The equilibria of Eq. (4.5b) by itself are states which have droplets with alternating high and low pressures $\bar{\mathcal{P}}_k = \mathcal{P}_\pm$. For simplicity, consider solutions where all of the drops are initially equally-spaced with $\bar{\mathcal{X}}_{k+1} - \bar{\mathcal{X}}_k = 1$. Expanding (4.5b) about this state yields

$$\frac{\mathrm{d}\hat{X}_k}{\mathrm{d}\tau} = \gamma(-1)^k(\hat{X}_{k+1} - 2\hat{X}_k + \hat{X}_{k-1}), \tag{4.11}$$

where $\gamma = -\mathbb{K}|\mathcal{P}_+ - \mathcal{P}_-|/\ln(\mathbb{R}\mathcal{P}_k) > 0$. A similar "alternating" linear operator was examined in [34]. The parameter γ is $O(1)$ and depends weakly on k if $|\mathcal{P}_+ - \mathcal{P}_-|$ is small; we shall treat it as a constant. To estimate the dominant eigenvalue, consider the inner product (treating boundary conditions appropriately),

$$\left|\left(\frac{\mathrm{d}\hat{X}}{\mathrm{d}\tau}, \hat{X}\right)\right| = \gamma\left|\sum_{k=1}^{N}(-1)^k(\hat{X}_k\hat{X}_{k+1} + \hat{X}_k\hat{X}_{k-1} - 2\hat{X}_k^2)\right| = 2\gamma\left|\sum_{k=1}^{N}(-1)^k\hat{X}_k^2\right| \leq 2\gamma|(\hat{X}, \hat{X})|. \tag{4.12}$$

From this, the Rayleigh quotient gives the upper bound $\lambda \leq 2\gamma$ for the eigenvalues. This upper bound is actually realized for the dominant instability mode [34]

$$\hat{X}(\tau) = \{1, 0, -1, 0, \ldots\}\,\mathrm{e}^{2\gamma\tau}. \tag{4.13}$$

This mode describes a set of simultaneous symmetric three-drop pinch collisions, where pairs of larger drops ($\mathcal{P}_-$) impinge on their smaller neighbors ($\mathcal{P}_+$), see Fig. 13b.

An illustration of the different modes of coarsening behavior is given in Fig. 14. Tracks of the droplet evolutions obtained from (2.15) are shown for a large system at three different values of the coarsening number. When $\mathbb{K}$ is small, the spatial motion of drops is relatively weak and coarsening by collapse of every other drop proceeds as expected, see Fig. 14a. When $\mathbb{K}$ is large, the drops move rapidly compared to the evolution of their pressures and collisions/merging is strongly favored, see Fig. 14c. For intermediate values of $\mathbb{K}$, there is a continuous transition between the collision- and collapse-dominated coarsening regimes; Fig. 14b shows the dynamics with an equal number of both types of coarsening events. While we do not yet have a complete theory to describe the competition between the two coarsening modes at moderate $\mathbb{K}$, we ran a numerical study over a large range of parameters and random initial conditions in (2.15) to track the fraction of events governed by each of the two coarsening mechanisms. Fig. 15 shows the fraction of collisions that occurred in 1000 runs over a range of values for $\mathbb{K}$ and ϵ. Interestingly, the collision fraction can be approximately fit to a combination of the parameters,

$$F_{\mathrm{collide}}(\mathbb{K}, \epsilon) \approx 0.63\sqrt{\ln\left(\frac{\mathbb{K}}{9\sqrt{|\ln\epsilon|}}\right)}. \tag{4.14}$$

We interpret the $\ln\epsilon$ factor as representing an averaged influenced of the $\mathbb{R}$ parameter. The figure suggests a well-defined cut-off for collision events, for $\mathbb{K} < 9\sqrt{|\ln\epsilon|}$, all coarsening was given by collapse events. The transition to collision dominated behavior was less sharp, but could be estimated as $\mathbb{K} > 110\sqrt{|\ln\epsilon|}$.

4.3. Long-term scaling behavior of coarsening

To describe the long-term dynamics of coarsening, we make use of a probabilistic argument to estimate the long-time form of the *number density* of droplets in the system,
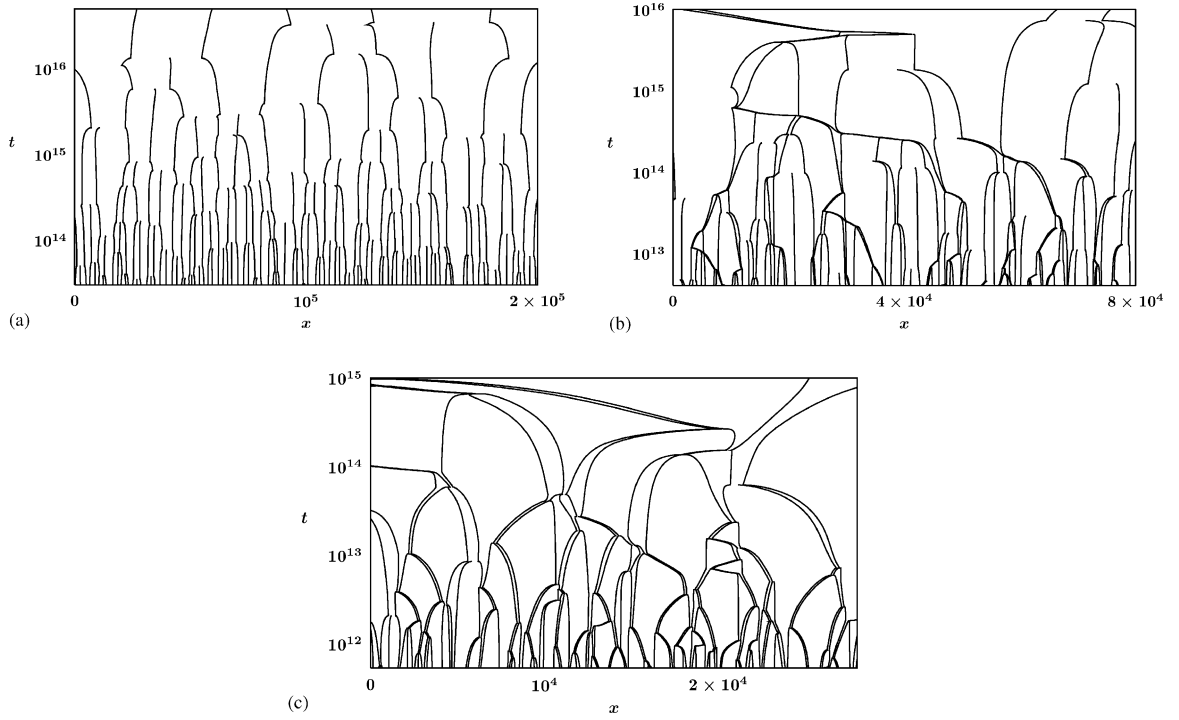
$$n(t) = \frac{N(t)}{L} \tag{4.15}$$

Fig. 14. Droplet evolution tracks for a system of 100 drops with $\epsilon = 0.01$ and at three different values of $\mathbb{K}$: (a) $\mathbb{K} = O(0.2/\epsilon)$, coarsening dominated by collapse events, (b) $\mathbb{K} = O(0.5/\epsilon)$, a balance between collapses and collisions, (c) $\mathbb{K} = O(1.5/\epsilon)$, collision dominated coarsening.

as $t \to \infty$. In [19], it was found that collapse-dominated coarsening follows a power-law scaling $N(t) = O(t^{-2/5})$. Here, we extend this result to obtain the dependence of the scaling coefficient on the system parameters, and consider the behavior for collision-dominated coarsening. This will be accomplished by considering the timescale of coarsening events in the rescaled system ((4.5a) and (4.5b)), and then restoring the original scalings.
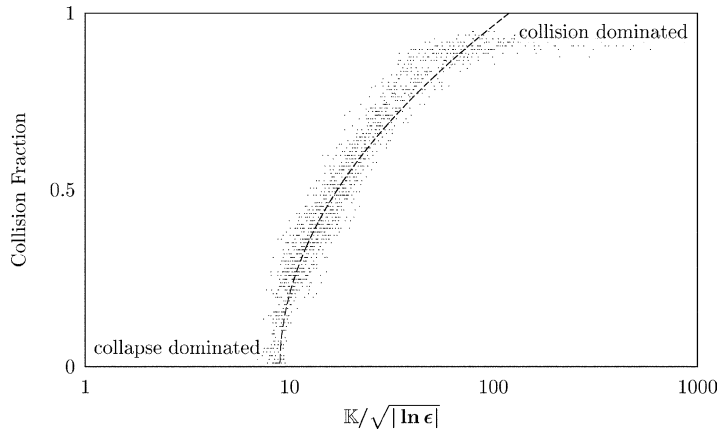

Fig. 15. Transition between collision- and collapse-dominated coarsening: the fraction of collisions as a function of the coarsening number $\mathbb{K}$ and ϵ sampled from 1000 runs with 100 drops each, on a range of $\mathbb{K}$ and $\epsilon = 10^{-j}$ for $j = 1$–4.

First, consider collapse-dominated coarsening ($\mathbb{K}/\ln(\mathbb{R})$ small), where the $\mathcal{X}_k$ vary slowly, so (4.5b) can be neglected and equations (4.5a) control the dynamics. Assume a very large array of drops, $N \gg 1$, and that each collapse event occurs independently of others. Since the collapse process is local, the time it takes a typical droplet to collapse, must be independent of the total number of drops. Consequently, the rate of decrease of n for each coarsening event must take the form,

$$\frac{1}{n}\frac{\mathrm{d}n}{\mathrm{d}\tau} = -\frac{1}{\tau_c} \tag{4.16}$$

where τ_c is the typical or average time between collapse events. The crucial observation is that τ_c is defined with respect to the rescaled system, and is therefore an $O(1)$ number independent of the number of droplets N. Reducing (4.5a) to a collapse model of the form (3.3), we can estimate $\tau_c \approx 1/6$. Using (4.1), (4.2) and (4.4) to restore scalings and explicitly express their n-dependence, this equation yields

$$\frac{\mathrm{d}n}{\mathrm{d}t} \approx -5.5836\epsilon^3 H_c^{-3/2} n^{7/2}, \tag{4.17}$$

with the solution

$$n(t) \approx (n(0)^{-5/2} + 13.959\epsilon^3 H_c^{-3/2}t)^{-2/5}. \tag{4.18}$$

Hence for $t \to \infty$, we obtain the power-law scaling in time, with the dependence on the coarsening number (4.7) and ϵ,

$$n(t) \propto \left(\frac{\mathbb{K}}{\epsilon}\right)^{3/5} t^{-2/5}. \tag{4.19}$$

Fig. 16 shows the collapse of results from simulations of coarsening at different values of $\mathbb{K}$ as predicted by (4.19).

A similar argument can be applied to collision-dominated coarsening, but there are some notable differences. We assume that droplet motion dominates the evolution (4.5b), so the $\mathcal{P}_k$ are held constant and (4.5a) is neglected. While collision events require the interaction of three drops, on the system-scale, they can still be modeled as independent local events when $N \gg 3$. Consequently, a similar collision coarsening rate law on the characteristic time-scale of (4.5b) can be written as

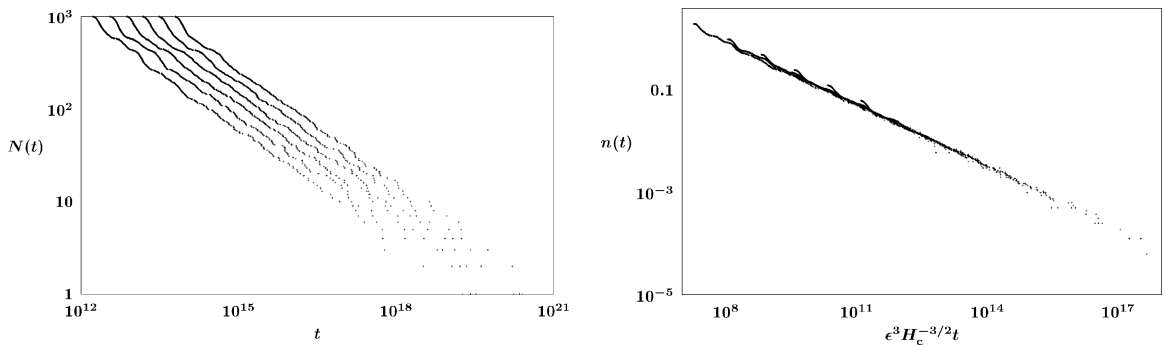$$\frac{1}{N}\frac{\mathrm{d}N}{\mathrm{d}\tau} \approx -\frac{\mathbb{K}}{\sigma_c|\ln\mathbb{R}|}, \tag{4.20}$$

Fig. 16. (Left) Plot of $N(t)$ from simulations of (2.15) at several values of $\mathbb{K} = O(0.2/[2^j\epsilon])$, for $j = 0, 1, 2, \ldots, 5$, and (right) the same data rescaled according to (4.19).
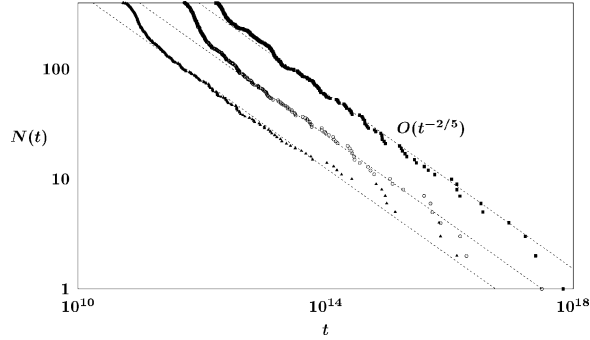
Fig. 17. $N(t)$ for the three simulations shown in Fig. 14 for $\mathbb{K}$ values in the collision, collapse and mixed coarsening regimes (solid dots) compared with the scaling law predicted by (4.22) (dotted lines).

where σ_c is an $O(1)$ collision time constant that could be bounded based on the analysis given in Section 3.3. This relation is on weaker footing than (4.16) since $\mathbb{R}$ evolves as coarsening proceeds, so the rate is not really independent of N, but the dependence is weak as it occurs through a logarithmic factor, so we will accept the need for logarithmic corrections to our expected power-law result. Similarly restoring the scalings in this equation yields

$$\frac{dn}{dt} \propto - \left(\frac{\mathbb{K}}{\sigma_c |\ln \mathbb{R}|} \right) \epsilon^3 H_c^{-3/2} n^{7/2}. \tag{4.21}$$

This leads to the approximate scaling law (apart from logarithmic corrections) for collision-dominated coarsening

$$n(t) \propto (\epsilon^3 \mathbb{K})^{1/5} t^{-2/5}. \tag{4.22}$$

It is interesting to note that both coarsening mechanisms yield the same 2/5 power-law for one-dimensional problems, but with different dependence on $\mathbb{K}$, ϵ. Fig. 17 shows that $N(t)$ for the three simulations from Fig. 14 in the collision, collapse, and mixed coarsening regimes all approximately follow this scaling law (with $n(t) = N(t)/L$).

5. Conclusions

The dynamics of the dewetting Eqs. (2.1) and (2.2) are remarkably rich. In contrast to the usual Cahn–Hilliard equation, isolated droplets (or "domains") can move substantially, allowing for collisions as an alternative coarsening mechanism. Additionally, the interaction of droplets is non-trivial: two droplets cannot directly merge in isolation, but can interact at a distance, whereas three drops may attract one another up to the point of binary collisions. As droplets become more mobile, the character of the system undergoes a transition from collision-dominated to mixed behavior at a very specific value of the control parameter $\mathbb{K}$; one may regard this as a "second-order phase transition" of this many-particle system.

It may be somewhat coincidental that both coarsening mechanisms give the same exponent 2/5 in one dimension. Indeed, Limary and Green [25] argue that the experimentally observed difference in scaling exponents might result from a crossover from one type of coarsening mechanism to the other. We anticipate that forthcoming theoretical studies of late stage dewetting on two-dimensional substrates will provide a more realistic opportunity to compare with experiments.

Appendix A. Calculation of the drift coefficient $C_X(\bar{p})$

We describe the details of the calculation of the drift coefficient function $C_X(\bar{p})$ (2.13). This coefficient can be expressed in terms of two integrals of the form

$$I_k(\bar{p}) \equiv \int_0^\infty \frac{(\bar{h} - h_{\min})^k}{\bar{h}^3} \, \mathrm{d}x, \tag{A.1}$$

as $C_X(\bar{p}) = \frac{1}{2} I_1(\bar{p})/I_2(\bar{p})$. These integrals are defined over a range of pressures $0 \le \bar{p} < p_{\max}$. We will consider the analysis for the limits $\bar{p} \to 0$ and $\bar{p} \to p_{\max}$, corresponding to very large and very small droplets, respectively.

Since $\bar{h}(x)$ is the homoclinic solution of (2.6) (Fig. 18), we can equivalently express these integrals as

$$I_k(\bar{p}) = \int_{h_{\min}}^{h_{\max}} \frac{(\bar{h} - h_{\min})^k}{\bar{h}^3 \sqrt{2R(\bar{h})}} \, \mathrm{d}\bar{h} \tag{A.2}$$

where $\bar{h}(x)$ satisfies

$$\frac{1}{2} \left(\frac{\mathrm{d}\bar{h}}{\mathrm{d}x} \right)^2 = R(\bar{h}), \tag{A.3}$$

with

$$R(\bar{h}) \equiv U(\bar{h}) - U(h_{\min}) - \bar{p}(\bar{h} - h_{\min}). \tag{A.4}$$

The minimum of the droplet profile $h_{\min}$ is a hyperbolic saddle point defined by $U'(h_{\min}) = \bar{p}$ and $h_{\max}$, the maximum of $\bar{h}(x)$, is defined by $R(h_{\max}) = 0$. For large and small droplets these quantities have the limits:

$$h_{\min}(\bar{p}) \sim \begin{cases} \epsilon(1 + O(\epsilon\bar{p})) & \bar{p} \to 0, \\ h_{\text{peak}} - O(\epsilon\sqrt{\epsilon[p_{\max} - \bar{p}]}) & \bar{p} \to p_{\max}, \end{cases} \tag{A.5}$$
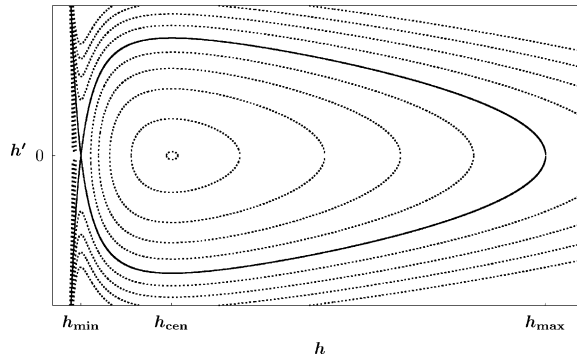

Fig. 18. The phase plane for Eq. (2.6) at a value of $\bar{p}$ in the range $0 < \bar{p} < p_{\max}$. The droplet solution is given by the homoclinic orbit to $h_{\min}(\bar{p})$ (solid curve).

$$h_{\max}(\bar{p}) \sim \begin{cases} \bar{p}^{-1}(-U(\epsilon) + \epsilon\bar{p} + O([\epsilon\bar{p}]^2)) & \bar{p} \to 0, \\ h_{\text{peak}} + O(\epsilon\sqrt{\epsilon[p_{\max} - \bar{p}]}) & \bar{p} \to p_{\max}, \end{cases} \tag{A.6}$$

where $h_{\text{peak}} = O(\epsilon)$ is the value of h corresponding to the maximum pressure, $U'(h_{\text{peak}}) = p_{\max}$. The elliptic center point of (2.6), $h_{\text{cen}} = O(\epsilon)$, is the other real root of $U'(\bar{h}) = \bar{p}$ and has the limiting behaviors,

$$h_{\text{cen}}(\bar{p}) \sim \begin{cases} \epsilon(\epsilon\bar{p} + (\epsilon\bar{p})^{m/n})^{-1/n} & \bar{p} \to 0, \\ h_{\text{peak}} + O(\epsilon\sqrt{\epsilon[p_{\max} - \bar{p}]}) & \bar{p} \to p_{\max}. \end{cases} \tag{A.7}$$

The dominant contributions to the value of (A.2) can be expected to come from the behavior of the integrand near the roots of $R(\bar{h})$. The local structure of $R(\bar{h})$ at its roots is given by

$$R(\bar{h}) \sim \begin{cases} \dfrac{1}{2}U''(h_{\min})(\bar{h} - h_{\min})^2 & \bar{h} \to h_{\min}, \\ [\bar{p} - U'(h_{\max})](h_{\max} - \bar{h}) & \bar{h} \to h_{\max}. \end{cases} \tag{A.8}$$

To evaluate $I_2(\bar{p})$, we note that as $\bar{h} \to h_{\min}$ the integrand vanishes, hence the integral depends only weakly on the structure of $R(\bar{h})$ there. Consequently, we use (A.8) for $\bar{h} \to h_{\max}$ to provide a global estimate, $R(\bar{h}) \leq [\bar{p} - U'(h_{\max})](h_{\max} - \bar{h})$, and estimate the integral by

$$I_2(\bar{p}) \approx \frac{1}{\sqrt{2|\bar{p} - U'(h_{\max})|}} \int_{h_{\min}}^{h_{\max}} \frac{(\bar{h} - h_{\min})^2}{\bar{h}^3\sqrt{h_{\max} - \bar{h}}}\, d\bar{h}. \tag{A.9}$$

Integrals of this form can be obtained in closed form as

$$\int_a^b \frac{(x-a)^2}{x^3\sqrt{b-x}}\, dx = -\frac{6b - 3a}{4b^2}\sqrt{b-a} + \frac{8b^2 - 8ab + 3a^2}{4b^{5/2}}\text{arctanh}(\sqrt{1 - a/b}). \tag{A.10}$$

Using the asymptotics for $h_{\min}, h_{\max}$, the limiting behaviors of (A.9) are given by

$$I_2(\bar{p}) \approx \begin{cases} -A_2\ln(\epsilon\bar{p}) - B_2 & \bar{p} \to 0, \\ C_2[\epsilon(p_{\max} - \bar{p})]^{3/4} & \bar{p} \to p_{\max}, \end{cases} \tag{A.11}$$

where the constants are $O(1)$ and depend only on the structure of the potential function $\mathcal{U}(H)$.

To estimate $I_1(\bar{p})$, we note that for $\bar{h} \to h_{\min}$ the ratio $(\bar{h} - h_{\min})/\sqrt{2R(\bar{h})}$ approaches a positive constant. Consequently, for $h_{\min} \to 0$, the $1/\bar{h}^3$ factor makes the integrand relatively large there. This contribution, along with the contribution for $\bar{h} \to h_{\max}$ lead to the estimate,

$$I_1 \approx \frac{1}{\sqrt{U''(h_{\min})}} \int_{h_{\min}}^{h_{\text{cen}}} \frac{d\bar{h}}{\bar{h}^3} + \frac{1}{\sqrt{2|\bar{p} - U'(h_{\max})|}} \int_{h_{\min}}^{h_{\max}} \frac{\bar{h} - h_{\min}}{\bar{h}^3\sqrt{h_{\max} - \bar{h}}}\, d\bar{h}, \tag{A.12}$$

where h_{cen} yields an effective cut-off for the influence of the behavior near $h_{\min}$. The first integral in (A.12) is straightforward; the second is of the form

$$\int_a^b \frac{x - a}{x^3\sqrt{b-x}}\, dx = \frac{2b - 3a}{4ab^2}\sqrt{b-a} + \frac{4b - 3a}{4b^{5/2}}\text{arctanh}(\sqrt{1 - a/b}). \tag{A.13}$$

Using the asymptotics for $h_{\min}, h_{\max}$, the limiting behaviors of (A.12) are given by

$$I_1(\bar{p}) \approx \begin{cases} \epsilon^{-1}[A_1 + B_1\epsilon\bar{p} + C_1\epsilon\bar{p}\ln(\epsilon\bar{p})] & \bar{p} \to 0, \\ D_1\epsilon^{-1}[\epsilon(p_{\max} - \bar{p})]^{1/4} & \bar{p} \to p_{\max}. \end{cases} \tag{A.14}$$

Therefore, the limiting behaviors of $C_X(\bar{p})$ are

$$C_X(\bar{p}) \approx \begin{cases} O([\epsilon\ln(\epsilon\bar{p})]^{-1}) & \bar{p} \to 0, \\ O([\epsilon^3(p_{\max} - \bar{p})]^{-1/2}) & \bar{p} \to p_{\max}. \end{cases} \tag{A.15}$$

Using a calculation similar to (A.9) for $I_2(\bar{p})$, we can also re-derive the result for the droplet mass. The mass of a droplet "core region" can be over-estimated by

$$M \approx 2\bar{w}h_{\min} + 2\int_0^\infty (\bar{h} - h_{\min})\,\mathrm{d}x. \tag{A.16}$$

Using (A.3) and (A.8) this can be written as

$$M \approx 2\bar{w}h_{\min} + \frac{2}{\sqrt{2[\bar{p} - U'(h_{\max})]}}\int_{h_{\min}}^{h_{\max}} \frac{\bar{h} - h_{\min}}{\sqrt{h_{\max} - \bar{h}}}\,\mathrm{d}\bar{h}. \tag{A.17}$$

Like (A.10) and (A.13) this integral can be found explicitly,

$$\int_a^b \frac{x - a}{\sqrt{b - x}}\,\mathrm{d}x = \frac{4}{3}(b - a)^{4/3}, \tag{A.18}$$

consequently, we obtain that the droplet mass as

$$M \sim \frac{2}{3}\frac{|2U(\epsilon)|^{3/2}}{\bar{p}^2} + O(\epsilon/\bar{p}) \qquad \bar{p} \to 0, \tag{A.19}$$

in agreement with the result (2.9).

References

[1] J. Becker, G. Grun, R. Seemann, H. Mantz, K. Jacobs, K.R. Mecke, R. Blossey, Complex dewetting scenarios captured by thin-film models, Nat. Mater. 2 (1) (2003) 59–63.
[2] G. Reiter, Dewetting of thin polymer films, Phys. Rev. Lett. 68 (1) (1992) 75–78.
[3] A. Sharma, R. Khanna, Pattern formation in unstable thin liquid films, Phys. Rev. Lett. 81 (16) (1998) 3463–3466.
[4] A. Sharma, R. Khanna, Pattern formation in unstable thin liquid films under the influence of antagonistic short- and long-range forces, J. Chem. Phys. 110 (10) (1999) 4929–4936.
[5] R. Xie, A. Karim, J.F. Douglas, C.C. Han, R.A. Weiss, Spinodal dewetting of thin polymer films, Phys. Rev. Lett. 81 (6) (1998) 1251–1254.
[6] J. Bischof, D. Scherer, S. Herminghaus, P. Leiderer, Dewetting modes of thin metallic films: nucleation of holes and spinodal dewetting, Phys. Rev. Lett. 77 (8) (1996) 1536–1539.
[7] A. Ghatak, R. Khanna, A. Sharma, Dynamics and morphology of holes in dewetting thin films, J. Coll. Int. Sci. 212 (1999) 483–494.
[8] U. Thiele, M.G. Velarde, K. Neuffer, Y. Pomeau, Film rupture in the diffuse interface model coupled to hydrodynamics, Phys. Rev. E 64 (3) (2001) 031602.
[9] U. Thiele, M.G. Velarde, K. Neuffer, Dewetting: film rupture by nucleation in the spinodal regime, Phys. Rev. Lett. 87 (1) (2001) 016104.
[10] R. Seemann, S. Herminghaus, K. Jacobs, Dewetting patterns and molecular forces: a reconcilation, Phys. Rev. Lett. 86 (24) (2001) 5534–5537.
[11] R.A. Segalman, P.F. Green, Dynamics of rims and the onset of spinodal dewetting at liquid/liquid interfaces, Macromolecules 32 (1999) 801–807.

[12] V. Mitlin, N.V. Petviashvilli, Nonlinear dynamics of dewetting: kinetically stable structures, Phys. Lett. A 192 (1994) 323.

[13] A.L. Bertozzi, G. Grun, T.P. Witelski, Dewetting films: bifurcations and concentrations, Nonlinearity 14 (6) (2001) 1569–1592.

[14] J.W. Cahn, J.E. Hilliard, Free energy of a nonuniform system. I: Interfacial free energy, J. Chem. Phys. 28 (1957) 258–267.

[15] R.L. Pego, Front migration in the nonlinear Cahn–Hilliard equation, Proc. R. Soc. Lond. A 422 (1989) 261–278.

[16] V.S. Mitlin, Dewetting of a solid surface: analogy with spinodal decomposition, J. Coll. Int. Sci. 156 (1993) 491–497.

[17] V.S. Mitlin, N.V. Petviashvili, Nonlinear dynamics of dewetting: kinetically stable structures, Phys. Lett. A 192 (1994) 323–326.

[18] A. Oron, S.G. Bankoff, Dewetting of a heated surface by an evaporating liquid film under conjoining/disjoing pressures, J. Coll. Int. Sci. 218 (1999) 152–166.

[19] K.B. Glasner, T.P. Witelski, Coarsening dynamics of dewetting films, Phys. Rev. E 67 (2003) 016302.

[20] P.W. Voorhees, The theory of Ostwald ripening, J. Stat. Phys. 38 (1–2) (1985) 231–252.

[21] I.M. Lifshitz, V.V. Slyozov, The kinetics of precipitation from supersaturated solid solutions, J. Chem. Phys. Solids 19 (1961) 35–50.

[22] C. Wagner, Theorie for alterung von niederschlagen durch umlosen, Z. Elektrochem. 65 (1961) 581–594.

[23] B. Niethammer, R.L. Pego, On the initial-value problem in the Lifshitz–Slyozov–Wagner theory of Ostwald ripening, SIAM J. Math. Anal. 31 (3) (2000) 467–485 (electronic).

[24] B. Niethammer, F. Otto, Domain coarsening in thin films, Comm. Pure Appl. Math. 54 (3) (2001) 361–384.

[25] R. Limary, P.F. Green, Dynamics of droplets on the surface of a structured fluid film: late-stage coarsening, Langmuir 19 (6) (2003) 2419–2424.

[26] P.G. de Gennes, Wetting: statics and dynamics, Rev. Mod. Phys. 57 (1985) 827–880.

[27] A. Oron, S.H. Davis, S.G. Bankoff, Long-scale evolution of thin liquid films, Rev. Mod. Phys. 69 (3) (1997) 931–980.

[28] L.M. Pismen, Y. Pomeau, Disjoining potential and spreading of thin liquid layers in the diffuse-interface model coupled to hydrodynamics, Phys. Rev. E 62 (2000) 2480–2492.

[29] L.W. Schwartz, Unsteady simulation of viscous thin-layer flows, in: Free Surface Flows with Viscosity, Computational Mechanics Publications, Boston, 1997, pp. 203–233.

[30] M.B. Williams, S.H. Davis, Nonlinear theory of film rupture, J. Coll. Int. Sci. 90 (1982) 220–228.

[31] J.P. Burelbach, S.G. Bankoff, S.H. Davis, Nonlinear stability of evaporating/condensing liquid films, J. Fluid Mech. 195 (1988) 463–494.

[32] K.B. Glasner, Spreading of droplets under the influence of intermolecular forces, Phys. Fluids 15 (7) (2003) 1837–1842.

[33] J.N. Israelachvili, Intermolecular and Surface Forces, Academic Press, New York, 1992.

[34] S.J. Watson, F. Otto, B.Y. Rubinstein, S.H. Davis, Coarsening dynamics of the convective Cahn–Hilliard equation, Physica D 178 (3–4) (2003) 127–148.

[35] E.K.O. Hellen, J. Krug, Coarsening of sand ripples in mass transfer models, Phys. Rev. E 66 (2002) 011304–9.

[36] U. Thiele, Open questions and promising new fields in dewetting, Euro. Phys. J. E 12 (3) (2003) 409–414.

[37] Michael J. Ward, Dynamic metastability and singular perturbations, in: Boundaries, Interfaces, and Transitions (Banff, AB, 1995), pp. 237–263. Amer. Math. Soc., Providence, RI, 1998.

[38] T.P. Witelski, D.G. Schaeffer, M. Shearer, A discrete model for an ill-posed nonlinear parabolic PDE, Physica D 160 (3–4) (2001) 189–221.